arXiv:1108.6075v1 [astro-ph.CO] 30 Aug 2011

# A CANDELS WFC3 GRISM STUDY OF EMISSION-LINE GALAXIES AT $Z \sim 2$: A MIX OF NUCLEAR ACTIVITY AND LOW-METALLICITY STAR FORMATION[*]

Jonathan R. Trump,[1] Benjamin J. Weiner,[2] Claudia Scarlata,[3] Dale D. Kocevski,[1] Eric F. Bell,[4] Elizabeth J. McGrath,[1] David C. Koo,[1] S. M. Faber,[1] Elise S. Laird,[5] Mark Mozena,[1] Cyprian Rangel,[5] Renbin Yan,[6] Hassen Yesuf,[1] Hakim Atek,[7] Mark Dickinson,[8] Jennifer L. Donley,[9] James S. Dunlop,[10] Henry C. Ferguson[9] Steven L. Finkelstein,[11] Norman A. Grogin,[9] Nimish P. Hathi,[12] Stéphanie Juneau,[2] Jeyhan S. Kartaltepe,[8] Anton M. Koekemoer,[9] Kirpal Nandra,[13] Jeffrey A. Newman,[14] Steven A. Rodney,[15] Amber N. Straughn,[16] and Harry I. Teplitz[7]

*Draft version September 1, 2011*

## ABSTRACT

We present *Hubble Space Telescope* Wide Field Camera 3 slitless grism spectroscopy of 28 emission-line galaxies at $z \sim 2$, in the GOODS-S region of the Cosmic Assembly Near-infrared Deep Extragalactic Legacy Survey (CANDELS). The high sensitivity of these grism observations, with $> 5\sigma$ detections of emission lines to $f > 2.5 \times 10^{-18}$ erg s$^{-1}$ cm$^{-2}$, means that the galaxies in the sample are typically $\sim 7$ times less massive (median $M_* = 10^{9.5} M_\odot$) than previously studied $z \sim 2$ emission-line galaxies. Despite their lower mass, the galaxies have [O III]/H$\beta$ ratios which are very similar to previously studied $z \sim 2$ galaxies and much higher than the typical emission-line ratios of local galaxies. The WFC3 grism allows for unique studies of spatial gradients in emission lines, and we stack the two-dimensional spectra of the galaxies for this purpose. In the stacked data the [O III] emission line is more spatially concentrated than the H$\beta$ emission line with 98.1% confidence. We additionally stack the X-ray data (all sources are individually undetected), and find that the average $L_{\rm [OIII]}/L_{0.5-10\rm keV}$ ratio is intermediate between typical $z \sim 0$ obscured active galaxies and star-forming galaxies. Together the compactness of the stacked [O III] spatial profile and the stacked X-ray data suggest that at least some of these low-mass, low-metallicity galaxies harbor weak active galactic nuclei.

*Subject headings:* galaxies: abundances — galaxies: active — quasars: emission lines — galaxies: evolution

## 1. INTRODUCTION

[1] University of California Observatories/Lick Observatory and Department of Astronomy and Astrophysics, University of California, Santa Cruz, CA 95064 USA
[2] Steward Observatory, University of Arizona, 933 North Cherry Avenue, Tucson, AZ 85721 USA
[3] Astronomy Department, University of Minnesota, Minneapolis, MN 55455 USA
[4] Department of Astronomy, University of Michigan, 500 Church St., Ann Arbor, MI 48109 USA
[5] Astrophysics Group, Imperial College London, Blackett Laboratory, Prince Consort Road, London SW7 2AZ UK
[6] Center for Cosmology and Particle Physics, Department of Physics, New York University, New York, NY 10003
[7] Spitzer Science Center, Caltech, Pasadena, CA 91125 USA
[8] National Optical Astronomical Observatories, Tucson, AZ 85719 USA
[9] Space Telescope Science Institute, 3700 San Martin Drive, Baltimore, MD 21218 USA
[10] Institute for Astronomy, University of Edinburgh, Royal Observatory, Edinburgh, EH9 3HJ UK
[11] Department of Physics and Astronomy, Texas A&M University, 4242 TAMU, College Station, TX 77843 USA
[12] Carnegie Observatories, 813 Santa Barbara Street, Pasadena, CA 91101 USA
[13] Max-Planck-Institut fr extraterrestrische Physik, Giessenbachstrasse 1, D-85748 Garching bei Mnchen, Germany
[14] Department of Physics and Astronomy, University of Pittsburgh, 3941 O'Hara St, Pittsburgh, PA 15260 USA
[15] Department of Physics and Astronomy, Johns Hopkins University, Baltimore, MD 21218 USA
[16] Astrophysics Science Division, Goddard Space Flight Center, Code 665, Greenbelt, MD 20771 USA

Rest-frame optical spectra contain a wealth of information about galaxy properties. In particular, the strengths and ratios between collisionally excited and recombination emission lines can be used to infer star formation rate (SFR, e.g. Kennicutt 1998), gas-phase metallicity (e.g. Kewley et al. 2001), and nuclear activity (e.g. Baldwin, Phillips & Terlevich 1981; Kewley et al. 2006). However applying these techniques to galaxies at higher redshifts is challenging for two reasons: (1) at $z > 1.5$ optical emission lines are observed in the near-infrared (NIR), where ground-based spectroscopy is challenging, and (2) the characteristics of $z > 1$ galaxies may be physically different from local galaxies.

The Wide Field Camera 3 (WFC3) G141 slitless grism on the *Hubble Space Telescope* (*HST*) addresses the first problem, with far improved capabilities for NIR spectroscopy than ground-based observatories (e.g., Straughn et al. 2011). Most of the previous ground-based studies of $z > 1.5$ galaxies have been biased to massive and UV-luminous systems (Shapley et al. 2004; Erb et al. 2006; Hayashi et al. 2009; Onodera et al. 2010), probably missing most of the more numerous, less massive galaxies at $1.5 < z < 3$. Only a handful of lower-mass galaxies at $z \sim 2$ have been studied, revealing much lower metallicities than both $z \sim 0$ galaxies of the same mass and their massive and evolved counterparts at the same redshift (Yuan & Kewley 2009; Erb et al. 2010; Finkelstein et al. 2011). In contrast the tremendous sensitivity of *HST*/WFC3 allows for $> 5\sigma$ detections of emission lines to $f > 2.5 \times 10^{-18}$ erg s$^{-1}$ cm$^{-2}$ for every object in a $2'.1 \times 2'.1$ field with 8 orbits. In addition, *HST* is
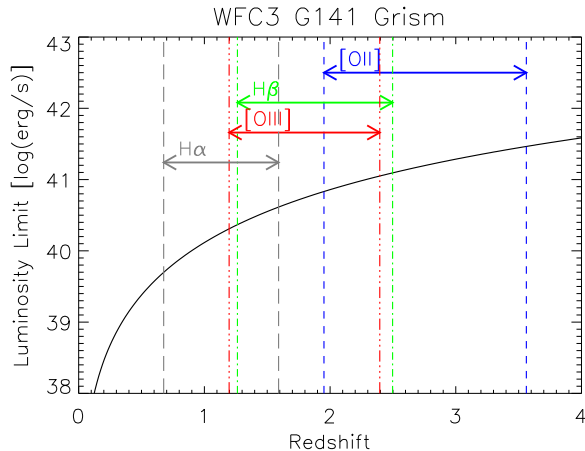
FIG. 1.— Line luminosity limits for detecting the Hα, Hβ, [O III], and [O II] emission lines with 8 orbits of the HST/WFC3 G141 grism (corresponding to a line flux limit of $2.5 \times 10^{-18}$ erg/s/cm$^2$). Dashed vertical lines indicate the redshift ranges at which each line is observed in the G141 wavelength range ($1.1 < \lambda < 1.7\mu m$). In this paper we study galaxies with Hβ and [O III] lines, selected at $1.3 < z < 2.4$.

not limited by atmospheric emission or absorption in the NIR, and so spectral lines are detectable over the entire 1.1-1.7 μm wavelength range of the WFC3 G141 grism. Figure 1 shows the detectability of emission lines with the G141 grism at various redshift ranges.

Star formation processes were quite different at $z > 1$ than in the local universe (e.g. Papovich et al. 2005; Reddy et al. 2006; Shim et al. 2011), and so it is not clear if the emission-line diagnostics used to characterize local galaxies can be directly applied to $z > 1$ systems. For example, the bulk of $z \sim 2$ galaxies have higher ratios of collisionally excited to recombination lines ([O III]/Hβ and [N II]/Hα) than local galaxies (Shapley et al. 2005b; Erb et al. 2006; Kriek et al. 2007). Local galaxies with high SFR tend to have higher emission-line ratios than galaxies with lower SFR, suggesting that rapid star formation leads to different ionization properties (Liu et al. 2008; Brinchmann, Pettini & Charlot 2008). Since $z > 1$ galaxies typically have higher SFR than local analogs of the same mass (e.g. Papovich et al. 2005), their higher line ratios may simply be the result of their higher SFR. However Wright et al. (2010) used spatially resolved spectroscopy of one galaxy at $z = 1.6$ to show that these line ratios increase in the center of the galaxy, with normal star-forming (SF) line ratios at outer apertures. This suggests that weak or obscured active galactic nucleus (AGN) activity may be the cause of higher line ratios in $z \sim 2$ galaxies, perhaps because AGN activity is correlated with SFR as observed locally (Kauffmann et al. 2003; Shi et al. 2009). There are many predictions for the density of obscured and Compton-thick (CT, $N_H \gtrsim 10^{24}$ cm$^2$) AGNs at $1.5 < z < 3$ from the X-ray background (Gilli et al. 2007; Treister et al. 2009) and from IR-excess galaxy counts and X-ray stacking (Daddi et al. 2007; Martinez-Sansigre et al. 2007; Fiore et al. 2009; Georgantopoulos et al. 2011), but to date only three CT AGNs have been individually confirmed at $z \sim 2$ (Alexander et al. 2005; Erlund et al. 2008; Alexander et al. 2008). Obscured AGNs are missed by even the deepest X-ray surveys, but can still ex-

hibit the narrow emission-line signature of an AGN (e.g., LaMassa et al. 2011). Measuring the density of obscured AGNs at $z \sim 2$ is especially important to reveal how much black hole growth occurs in an enshrouded phase.

Here we use 8.5 orbits of WFC3 G141 spectroscopy to study the properties of emission-line galaxies at $1.3 < z < 2.4$ in the Hubble Ultra Deep Field (HUDF, Beckwith et al. 2006). These data were taken as part of the supernova follow-up program in the Cosmic Assembly Near-Infrared Deep Extragalactic Legacy Survey (CANDELS[18], Grogin et al. 2011; Koekemoer et al. 2011). The supernova candidate identified in the HUDF region is described by Rodney et al. (2011), and this work makes use of the spectra that were serendipitously obtained for hundreds of other targets in the $2.1' \times 2.1'$ field. In particular we focus on the 28 galaxies exhibiting Hβ and [O III] emission lines in the observed grism wavelength range (at $1.3 < z < 2.4$). Like the study by Wright et al. (2010), the high spatial resolution of the HST/WFC3 similarly allows for studies of spatial gradients in emission-line properties. Unlike an integral field unit spectrograph, however, the WFC3 grism has the unique ability to do this for hundreds of objects in the field of view simultaneously.

In §2 we describe the observations, data reduction, and emission line luminosity limits. In §3 we describe our method for calculating emission lines, complicated by the limited spectral resolution of the WFC3 G141 grism. In §4 we stack the spatially resolved spectra to show that both the emission-line properties and the stacked X-ray data are suggestive of weak AGN activity in at least some of these galaxies. We summarize our results in §5. Throughout the paper we adopt a cosmology with $h = 0.70$, $\Omega_M = 0.3$, $\Omega_\Lambda = 0.7$.

## 2. HST/WFC3 SLITLESS GRISM OBSERVATIONS

The HUDF was observed with the HST/WFC3 G141 grism on 26-27 Oct 2010 and 1 Nov 2010 for a total of 8.5 orbits. The data were acquired in two different orients, with 2.5 orbits at an orient of $PA = 176°$ on the sky and 6 orbits at an orient of $PA = 182.4°$. The data for each orient were reduced using the aXe software (Kümmel et al. 2009, available at http://axe.stsci.edu/axe/), which flux- and wavelength-calibrated the data and provided co-added two-dimensional (2D) spectra as well as optimally extracted one-dimensional (1D) spectra. The usable wavelength range of each reduced spectrum is $1.1 < \lambda < 1.7\mu m$, with a resolution of $R \simeq 130$ (46.5Å/pixel for a point source and $0.''13$/pixel).

The G141 grism is slitless, and this introduces a number of complexities when interpreting the data. Spatially extended sources have features which appear extended in the wavelength direction, and so broad emission or absorption lines can be caused by either large velocity widths or by the size of the object. In addition, spectra frequently suffer from contamination by 0th order, 1st order, and 2nd order spectra of nearby sources. For this reason we did not combine the two orients, instead analyzing each orient independently and using them to identify contamination.

We calculated redshifts for all 455 targets detected in the HUDF G141 data. The best redshift was found

using a cross-correlation template-fitting IDL algorithm based on the publicly available `idlspec2d` package written by D. Schlegel[19]. Previous spectroscopic redshifts (Wolf et al. 2004; Mignoli et al. 2005; Vanzella et al. 2008; Straughn et al. 2008) and photometric redshifts (Wolf et al. 2004; Grazian et al. 2006; Ryan et al. 2007; Wuyts et al. 2008; Cardamone et al. 2010) were used as priors. We used two templates: a star-forming emission-line galaxy and a passive absorption line galaxy. Each template was constructed using the high-resolution optical ($3800 < \lambda < 9200$Å) templates from the SDSS library[20] combined with supplemental low-resolution UV and NIR data from the SWIRE photometric templates (Polletta et al. 2007), with the final templates resampled to match the spectral resolution of the WFC3 G141 data. All spectra and their redshift fits were visually inspected to ensure quality.

Of the 455 targets, we selected the 28 galaxies at $1.3 < z < 2.4$ and H$\beta$ or [O III] emission-line luminosities of $L > 1.8 \times 10^{41}$ erg s$^{-1}$. This luminosity limit represents the flux limit for detecting emission lines at the $5\sigma$ level ($f > 2.5 \times 10^{-18}$ erg s$^{-1}$) at $z = 2.4$. For all 28 galaxies we detect both H$\beta$ and [O III] in both grism pointings, and as a result their redshifts are unambiguous. Table 1 shows the properties of these 28 emission-line galaxies. Their median redshift is 1.86.

## 2.1. Stellar Masses and Rest-frame Colors

Rest-frame magnitudes and stellar masses were calculated from the GOODS-MUSIC photometry catalog (Santini et al. 2009) by fitting a set of template spectral energy distributions drawn from the PEGASE stellar population models (see Fioc & Rocca-Volmerange 1997 for a description of an earlier version of this stellar population model). We allow dust attenuation following Calzetti (2001), with values of $E(B-V)_{\rm gas}$ between -0.05 and 1.5. (Slightly negative $E(B-V)$ avoids biasing the mean properties of the population by accounting for the rare cases when photometric error gives fits that prefer slightly negative attenuation. In practice all of our emission-line galaxies have best-fit $E(B-V) > 0$ anyway.) All templates have solar metallicity, and included a broad range of exponentially-decreasing, constant, or exponentially-rising star formation beginning at $z_f \sim 4$. A grid of stellar population templates were compared with photometric data points of each galaxy, given the spectroscopic redshift from the grism data, and the best matching template was used to calculate rest-frame colors and a stellar $M/L$ ratio. Compared to galaxies with independently-estimated stellar masses (from independent photometry of similar but not identical datasets) in the GOODS-S field (Wuyts et al. 2008), our method yields similar masses for intensely star-forming galaxies both with and without dust attenuation (i.e., the galaxies of interest here), with a scatter of 0.3 dex. Our masses are 0.1-0.25 dex larger for moderately star-forming galaxies or non-star-forming galaxies because our templates include older stellar populations than those used by Wuyts et al. (2008). Rest-frame colors are reproduced to within 0.1 mag in rest-frame ($U - B$) color for all galaxy
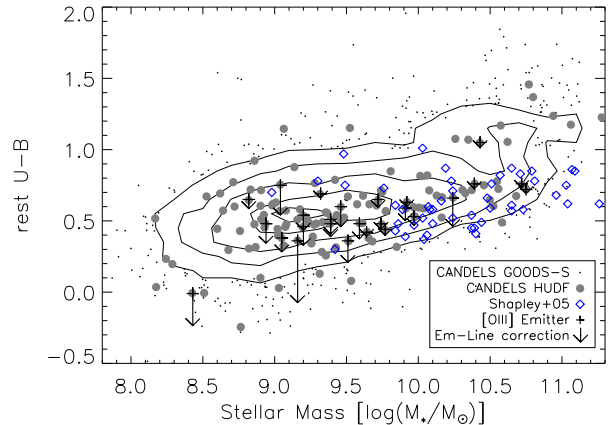
FIG. 2.— Rest-frame ($U - B$) color and stellar mass for our 28 emission-line galaxies (black crosses). Typical $1\sigma$ errors are $\sim 0.1$ magnitudes in ($U - B$) and $\sim 0.3$ dex in mass. For comparison filled gray circles show the 137 galaxies at $1.3 < z < 2.4$ in the HUDF and gray contours and points show the entire set of 4140 GOODS-S galaxies in the redshift range, both with masses and rest-frame quantities calculated from the same photometry and with the same method. Blue diamonds show a comparison sample of $z \sim 2$ galaxies from Shapley et al. (2005a): this is the parent sample of most previous studies of emission-line galaxies at $z \sim 2$. Arrows show the effects on ($U - B$) color if the H$\beta$ and [O III] emission lines are removed (although the [O II] emission line, which is not measured here, could have the opposite effect on ($U - B$) color). The WFC3 grism reveals galaxies with masses a factor of $\sim 7$ lower than previous studies of $z \sim 2$ emission-line galaxies.

types. Full details on the derived masses and rest-frame quantities are given by Bell et al. (in prep).

As shown by van der Wel et al. (2011), strong emission lines can have significant effects on broad-band colors in $z \sim 2$ galaxies. In our galaxies the median total equivalent width (EW) of the H$\beta$ and [O III] lines is $EW_{\rm obs} = 220$Å: this brightens the rest-frame $B$ magnitude by $\sim 20\%$ and reddens the ($U - B$) color by 0.2 magnitudes. Despite these effects, we do not correct rest-frame magnitudes for emission lines for two reasons. First, the [O II] emission line could have the opposite effect, brightening $U$ and causing $U - B$ to appear bluer, but we do not measure this emission line because it is not generally present in our observed spectral range. In addition, the SF/AGN diagnostic we use (Yan et al. 2011) was calibrated with ($U - B$) colors uncorrected for emission lines, and so we do not correct our colors to remain consistent.

Figure 2 shows the rest-frame ($U - B$) colors and stellar masses for our 28 emission-line galaxies. Also shown by gray filled circles are the 137 galaxies in the HUDF with photometric or spectroscopic redshifts at the same $1.3 < z < 2.4$, with rest-frame colors and stellar masses computed in an identical fashion. The emission-line galaxies studied here are rather common at $1.3 < z < 2.4$, making up $\sim 20\%$ of the total $H < 26$ galaxy population. Gray contours additionally show the set of all 4140 GOODS-S galaxies with photometric or spectroscopic redshifts in the same $1.3 < z < 2.4$ redshift range, and our galaxies have a roughly similar distribution of mass and slightly bluer colors than the larger parent distribution. For comparison with previous samples, we also show the 50 galaxies at $1.3 < z < 2.4$ of Shapley et al. (2005a), using their masses and

TABLE 1
HUDF WFC3/G141 Emission-Line Galaxies

| # | RA | Dec | $z$ | $H_{AB}$ | $\log(L_{H\beta})$ | $\log(L_{[OIII]})$ | $f_{[OIII]}/f_{H\beta}$ | $(U-B)_{rest}$ | $\log(M_*)$ | $f_{0.5-10keV}$ |
|---|---|---|---|---|---|---|---|---|---|---|
| - | [deg] | (J2000) | - | [mag] | [log(erg/s)] | [log(erg/s)] | - | [mag] | [log($M_\odot$)] | [$10^{-16}$ erg s$^{-1}$ cm$^{-2}$] |
| 1 | 53.135250 | -27.781778 | 1.44 | 22.67 | $41.08^{+0.28}_{-0.15}$ | $41.48^{+0.14}_{-0.12}$ | $2.52^{+0.77}_{-1.13}$ | 0.76 | 10.39 | < 0.45 |
| 2 | 53.141159 | -27.759295 | 1.77 | 24.19 | $40.89^{+0.21}_{-0.11}$ | $41.61^{+0.05}_{-0.05}$ | $5.23^{+1.22}_{-2.06}$ | 0.51 | 9.39 | < 0.44 |
| 3 | 53.143940 | -27.779781 | 1.71 | 25.21 | $40.92^{+0.25}_{-0.16}$ | $41.35^{+0.07}_{-0.21}$ | $2.97^{+0.18}_{-1.77}$ | 0.38 | 9.05 | < 0.47 |
| 4 | 53.144127 | -27.773602 | 1.90 | 23.58 | $41.18^{+0.11}_{-0.18}$ | $41.92^{+0.05}_{-0.02}$ | $5.54^{+2.72}_{-1.14}$ | 0.36 | 9.51 | < 0.44 |
| 5 | 53.144485 | -27.791162 | 1.42 | 23.52 | $40.97^{+0.28}_{-0.02}$ | $41.93^{+0.05}_{-0.05}$ | $8.09^{+1.05}_{-3.35}$ | 0.46 | 9.20 | < 0.46 |
| 6 | 53.144840 | -27.778469 | 2.22 | 24.37 | $41.10^{+0.23}_{-0.06}$ | $41.95^{+0.02}_{-0.06}$ | $7.10^{+1.45}_{-3.24}$ | 1.00 | 9.28 | < 0.47 |
| 7 | 53.146435 | -27.778353 | 1.87 | 24.74 | $41.18^{+0.10}_{-0.22}$ | $41.94^{+0.01}_{-0.09}$ | $5.74^{+2.62}_{-1.61}$ | -0.01 | 8.43 | < 0.47 |
| 8 | 53.146900 | -27.781837 | 1.55 | 24.09 | $40.74^{+0.23}_{-0.14}$ | $41.27^{+0.10}_{-0.13}$ | $3.35^{+0.97}_{-1.51}$ | 0.48 | 9.39 | < 0.46 |
| 9 | 53.147469 | -27.777693 | 1.83 | 22.80 | $40.83^{+0.33}_{-0.05}$ | $41.57^{+0.06}_{-0.10}$ | $4.52^{+1.11}_{-2.15}$ | 1.05 | 10.43 | < 0.47 |
| 10 | 53.147747 | -27.765675 | 2.31 | 23.75 | $41.08^{+0.28}_{-0.08}$ | $41.70^{+0.21}_{-0.01}$ | $4.22^{+1.96}_{-1.61}$ | 0.59 | 9.91 | < 0.43 |
| 11 | 53.147804 | -27.771420 | 2.17 | 24.52 | $41.36^{+0.07}_{-0.28}$ | $42.01^{+0.04}_{-0.09}$ | $5.09^{+2.35}_{-1.24}$ | 0.65 | 8.82 | < 0.45 |
| 12 | 53.148003 | -27.787737 | 1.90 | 23.80 | $40.96^{+0.31}_{-0.11}$ | $41.24^{+0.19}_{-0.16}$ | $2.02^{+0.35}_{-1.09}$ | 0.63 | 9.92 | < 0.45 |
| 13 | 53.149063 | -27.785116 | 2.07 | 24.20 | $41.02^{+0.25}_{-0.23}$ | $41.38^{+0.10}_{-0.23}$ | $1.90^{+1.28}_{-0.88}$ | 0.65 | 9.72 | < 0.44 |
| 14 | 53.151283 | -27.792444 | 1.86 | 24.05 | $41.18^{+0.30}_{-0.05}$ | $41.74^{+0.15}_{-0.04}$ | $3.62^{+0.77}_{-1.62}$ | 0.48 | 9.59 | < 0.43 |
| 15 | 53.151691 | -27.763506 | 2.16 | 25.19 | $40.55^{+0.39}_{-0.04}$ | $41.24^{+0.03}_{-0.33}$ | $2.88^{+1.06}_{-1.80}$ | 0.48 | 8.94 | < 0.44 |
| 16 | 53.152264 | -27.770132 | 1.85 | 23.21 | $41.26^{+0.13}_{-0.24}$ | $41.77^{+0.06}_{-0.04}$ | $3.23^{+2.34}_{-0.88}$ | 0.53 | 9.97 | < 0.47 |
| 17 | 53.152870 | -27.772545 | 1.85 | 24.13 | $41.29^{+0.03}_{-0.21}$ | $41.95^{+0.03}_{-0.04}$ | $5.52^{+1.58}_{-1.36}$ | 0.36 | 9.16 | < 0.46 |
| 18 | 53.152874 | -27.780163 | 1.86 | 24.33 | $40.65^{+0.26}_{-0.12}$ | $41.32^{+0.01}_{-0.21}$ | $3.73^{+0.90}_{-1.72}$ | 0.60 | 9.46 | < 0.46 |
| 19 | 53.153774 | -27.767345 | 2.32 | 23.65 | $40.98^{+0.22}_{-0.16}$ | $41.58^{+0.11}_{-0.11}$ | $3.94^{+1.50}_{-1.61}$ | 0.44 | 9.77 | < 0.46 |
| 20 | 53.154453 | -27.771494 | 2.23 | 22.76 | $41.67^{+0.14}_{-0.09}$ | $42.49^{+0.13}_{-0.06}$ | $6.63^{+1.01}_{-2.31}$ | 0.66 | 10.24 | < 0.46 |
| 21 | 53.155643 | -27.779324 | 1.85 | 22.10 | $41.60^{+0.22}_{-0.18}$ | $41.83^{+0.13}_{-0.12}$ | $1.27^{+1.33}_{-0.32}$ | 0.76 | 10.72 | < 0.45 |
| 22 | 53.156372 | -27.767874 | 2.02 | 24.07 | $40.75^{+0.34}_{-0.05}$ | $41.23^{+0.12}_{-0.20}$ | $2.61^{+0.31}_{-1.39}$ | 0.83 | 9.19 | < 0.47 |
| 23 | 53.157207 | -27.778561 | 1.31 | 23.86 | $40.94^{+0.31}_{-0.15}$ | $41.45^{+0.08}_{-0.28}$ | $3.17^{+0.01}_{-1.88}$ | 0.54 | 9.20 | < 0.45 |
| 24 | 53.160435 | -27.775246 | 1.41 | 20.86 | $41.08^{+0.19}_{-0.26}$ | $41.34^{+0.07}_{-0.04}$ | $1.81^{+1.34}_{-0.62}$ | 0.42 | 9.64 | < 0.46 |
| 25 | 53.160446 | -27.790394 | 1.61 | 23.44 | $41.23^{+0.15}_{-0.50}$ | $41.57^{+0.07}_{-0.12}$ | $1.39^{+4.25}_{-0.11}$ | 0.48 | 9.74 | < 0.43 |
| 26 | 53.165157 | -27.781664 | 2.22 | 24.56 | $40.90^{+0.25}_{-0.15}$ | $41.60^{+0.07}_{-0.19}$ | $5.88^{+0.28}_{-3.79}$ | 0.69 | 9.32 | < 0.44 |
| 27 | 53.172153 | -27.763655 | 2.21 | 24.83 | $41.03^{+0.23}_{-0.23}$ | $41.79^{+0.14}_{-0.11}$ | $5.77^{+3.09}_{-1.84}$ | 0.75 | 9.04 | < 0.48 |
| 28 | 53.172241 | -27.760641 | 1.54 | 21.83 | $41.33^{+0.56}_{-0.07}$ | $41.65^{+0.19}_{-0.06}$ | $2.09^{+0.40}_{-1.44}$ | 0.72 | 10.75 | < 0.48 |

$(U-B)$ colors calculated from their photometry using the publicly available `kcorrect` package (Blanton & Roweis 2007). The galaxies of Shapley et al. (2005a) form the parent sample for most previous $z \sim 2$ emission-line studies (e.g., Shapley et al. 2005b; Erb et al. 2006, 2010; Wright et al. 2010). The median mass of the grism galaxies is $M_* \sim 10^{9.5} M_\odot$, a factor of $\sim 7$ lower than the median mass of the Shapley et al. (2005a) sample. Several of the emission-line galaxies from the WFC3 grism data appear to be star-forming dwarf galaxies with masses of only $M_* \sim 10^9 M_\odot$.

### 2.2. X-ray Data

The HUDF has the deepest X-ray data in the sky, with 4 Ms of *Chandra* data. Imaging was obtained in 54 observations (obsIDs) over the course of 3 *Chandra* observing cycles in 2000, 2007 and 2010 using the Advanced CCD Imaging Spectrometer imaging array (ACIS-I Garmire et al. 2003). The data were reduced using CIAO v4.2 according to the basic procedure described in Laird et al. (2009). Before combining the observations, the astrometry of each obsID was registered to that of the GOODS-MUSYC survey (Gawiser et al. 2006) by matching the positions of bright X-Ray sources to H-band selected sources, using the tool `reproject_aspect`. Source detection was carried out according to the method described in Laird et al. (2009), and none of our galaxies

are detected. We instead assign $3\sigma$ upper limits calculated using the background and PSF size from the location of each galaxy on the *Chandra*/ACIS detector.

### 3. LINE MEASUREMENTS

Because the grism is slitless, any spatial extent along the dispersion direction will artificially broaden spectral features. The [OIII]$\lambda$4959 and [OIII]$\lambda$5007 lines are often completely blended together in resolved galaxies, and larger systems additionally have H$\beta\lambda$4861 partially blended with the two [OIII] lines. For this reason we do not attempt to individually measure each of the H$\beta$ [OIII] lines directly from the data. Instead we subtract a linear continuum in the region $4770 < \lambda < 5100$Å and fit the residual with a mixture of three Gaussians. The three Gaussians are constrained to be centered within 20Å ($\sim$1200 km s$^{-1}$) of 4861Å, 4959Å, and 5007Å, in the rest frame. Because the two [OIII] lines are blended, we measure the [OIII]$\lambda$5007 flux as 3/4 of the total [OIII] flux (i.e., 3/4 of the the sum of the two Gaussians centered near 4959Å and 5007Å; Storey & Zeippen 2000). Errors in line flux (and $f([OIII])/f(H\beta)$ and $L_{[OIII]}$) are calculated by bootstrapping 10 000 realizations of the resampled data.

Figure 3 shows the H$\beta$ and [OIII] line regions for eight emission-line galaxies. The 2D dispersed image, 1D spectrum, and line fit is shown for each object.
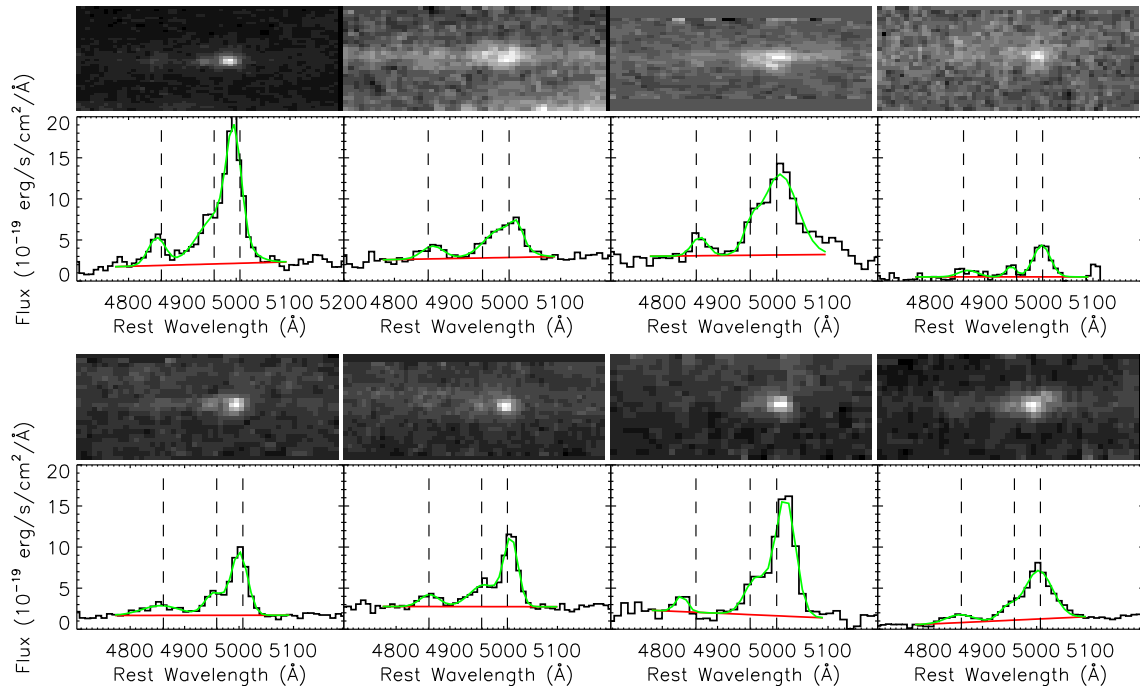
FIG. 3.— Examples of fits to the H$\beta$ and [O III] emission lines for eight of the emission-line galaxies. Dashed vertical lines indicate the line centers for the H$\beta\lambda$4861, [O III]$\lambda$4959, and [O III]$\lambda$5007 emission lines. Because the G141 grism has such low spectral resolution, the H$\beta$ and [O III] lines are frequently blended. We subtract the continuum, shown by the red line, and fit the entire system with a mixture of three Gaussians, shown by the green line. The [O III]$\lambda$5007 flux is measured as 3/4 of the total [O III] flux.

The classical "BPT" diagnostic (Baldwin, Phillips & Terlevich 1981) uses emission-line ratios (namely, $f([\text{O III}])/f(\text{H}\beta)$ and $f([\text{N II}])/f(\text{H}\alpha)$) to distinguish galaxies dominated by star formation or black hole activity in the local universe (see also Veilleux & Osterbrock 1987; Kewley et al. 2001). However in the WFC3 grism data, H$\alpha$ and [N II] are hopelessly blended, and additionally are redshifted beyond the observed grism redshift range at $z > 1.6$. Yan et al. (2011) showed that it is possible to construct an alternate version of the BPT diagnostic which replaces $f([\text{N II}])/f(\text{H}\alpha)$ with rest-frame $(U - B)$ color. This modified BPT diagnostic is especially useful for interpreting the WFC3 grism data.

An alternative SF/AGN classification diagnostic possible for our galaxies is the "MEx" diagram (Juneau et al. 2011), which replaces the $(U - B)$ color with stellar mass $M_*$. Stellar mass, however, is dependent on the physics of the model, and could be systematically inaccurate due to the constraints of available templates. Meanwhile rest-frame color does not depend on the physics of the model, only its goodness of fit to the data. For this reason we prefer $(U - B)$ over $M_*$, noting that the Yan et al. (2011) diagnostic agrees well with the "MEx" method (see Appendix A of Juneau et al. 2011).

Figure 4 shows our $z \sim 2$ emission-line galaxies on the modified BPT diagnostic of Yan et al. (2011), along with comparison samples at $z \sim 0$ and $z \sim 0.6$ (also from Yan et al. 2011) and $z \sim 1.2$ (from Liu et al. 2008). Galaxies dwelling on the left and bottom of each panel tend to be SF dominated, while systems in the upper right are AGN dominated. Low metallicity galaxies tend to have bluer colors and higher $f([\text{O III}])/f(\text{H}\beta)$ ratios, and indeed the locus of SF galaxies tends to shift to the upper left from $z \sim 0$ to $z \sim 0.6$ to $z > 1$. Our galaxies

generally lie in same region as previously studied $z > 1$ galaxies.

Directly interpreting the position of $z > 1$ galaxies on the modified BPT diagnostic in Figure 4 is challenging for several reasons, however. First, the dividing line of Yan et al. (2011) between SF galaxies and AGN was empirically calibrated at $z < 1$ only, and it is unclear if this dividing line changes with redshift. Local galaxies with higher SFR tend to have higher line ratios (Liu et al. 2008; Brinchmann, Pettini & Charlot 2008), and since $z \sim 2$ galaxies have higher SFR galaxies than local galaxies of similar mass (Papovich et al. 2005), we might already expect them to have a higher $f([\text{O III}])/f(\text{H}\beta)$ ratios from both their rapid star formation and low metallicity. On the other hand, active galaxies might also be more likely to be confused as SF-dominated in low-mass, low-metallicity galaxies. Izotov & Thuan (2008) showed that AGN accreting as high as the Eddington limit contribute less than 10% to the emission-line ratios in metal-poor dwarf galaxies. Our $z \sim 2$ galaxies have similarly low masses, and the emission from their low-mass black holes would be overwhelmed by a SFR of a few solar masses per year.

For these reason it is difficult to interpret the absolute position of objects, and more instructive to consider relative positions of the inner and outer regions of the galaxies, as well as differences in the profiles of [O III] and H$\beta$.

### 3.1. Stacked HST/WFC3 Data

The slitless WFC3 grism provides spatially resolved spectroscopy, with a scale of 0$\farcs$13 per pixel. This is particularly useful for studying gradients of emission-line ratios: most local galaxies have a higher ratio of $f([\text{O III}])/f(\text{H}\beta)$ in outer regions due to negative metal-

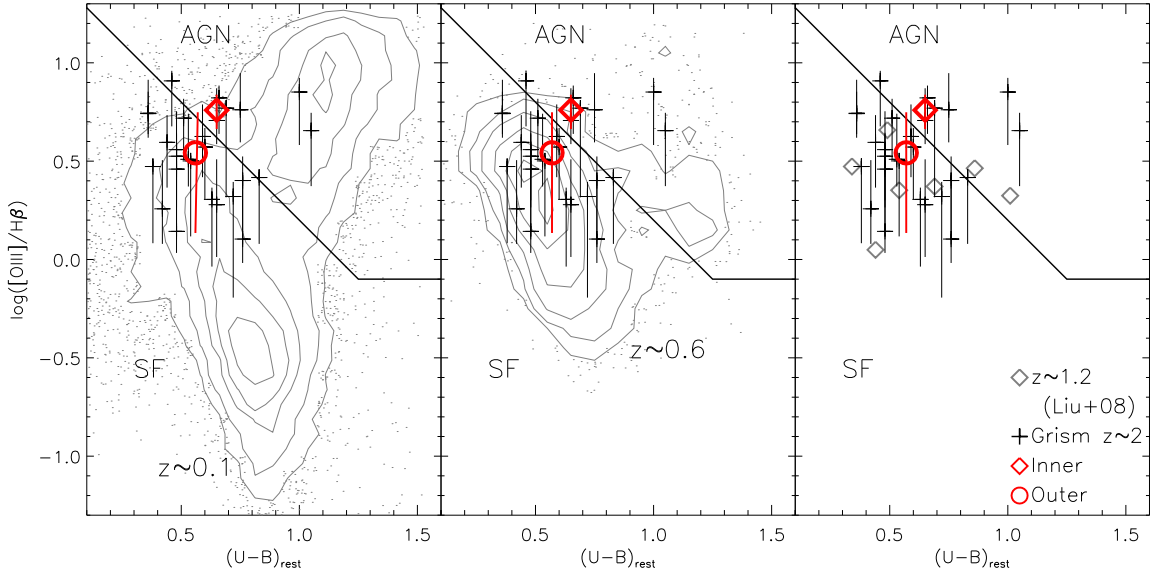Fig. 4.— Ratio of [O III] to Hβ with rest-frame $(U - B)$ color. The solid line shows the division between AGN (upper right) and star formation (left and bottom) from Yan et al. (2011). Crosses show the 28 $z \sim 2$ galaxies from the WFC3 G141 data. Contours and points show comparison samples (also from Yan et al. 2011) at $z \sim 0$ (left panel) and $z \sim 0.6$ (middle panel). In the right panel, gray diamonds show a comparison sample at $z \sim 1.2$ from Liu et al. (2008). The red points show the colors and line ratios of the stacked data: the diamond shows the inner $0.''39$ region and the circle shows the outer $0.''39 - 0.''78$ region. The $z \sim 0$ and $z \sim 0.6$ comparison samples have the same line luminosity constraint as the WFC3 G141 data, with either Hβ or [O III] of $L > 1.8 \times 10^{41}$ erg s$^{-1}$. From $z \sim 0.1$ to $z \sim 0.6$ to $z \sim 1.2$, galaxies have lower metallicities and consequently move to the upper left of the figure, and our $z \sim 2$ galaxies lie in very similar space to the previously studied $z \sim 1.2$ galaxies of Liu et al. (2008). The line ratio and color of the inner region of the stacked data is marginally $(1.0\sigma)$ more AGN-like than the outer region.

licity gradients (e.g., van Zee et al. 1998), while a higher ratio in a galaxy nucleus would suggest the presence of an AGN. In general the signal-to-noise (S/N) of our data is too low to measure line ratio gradients for individual galaxies; instead we stack the 2D spectroscopy to study line ratio gradients.

We stack the 2D images for each galaxy, equal-weighting each galaxy by normalizing its total (Hβ + [O III]λ4959 + [O III]λ5007) line emission. Images are aligned by the peak of the emission (dominated by the [O III]λ5007 line). This stacked spectrum allows us to study the spatial extent of the Hβ and [O III] emission lines.

One-dimensional spatial profiles can be constructed by extracting each emission line along the cross-dispersion direction. Figure 5 shows the spatial profiles for the Hβλ4861 and [O III]λ5007 emission lines, along with the collapsed cross-dispersion profile of the entire 2D spectrum. Each emission line is extracted from the central three pixels (140Å) about the line center. The Hβ line has a cross-dispersion full-width half-maximum (FWHM) of 7.2 pixels ($0.''94$, $\sim$8 kpc), while the [O III] line is narrower with a FWHM of 4.9 pixels ($0.''64$, $\sim$5 kpc).

We test the significance of the [O III] line being more spatially compact than the Hβ line by bootstrapping 100 000 resampled profiles. We construct each boot-strapped profile by adding a normally-distributed random error (with $\sigma$ given by the propagated error of the stacked profile) to the original data, and then measure FWHM([O III]) and FWHM(Hβ). The fraction of boot-strapped profiles with FWHM([O III])¡FWHM(Hβ) gives the significance of [O III] being more compact than Hβ. This occurs in 98.1% of the resampled data sets, and so
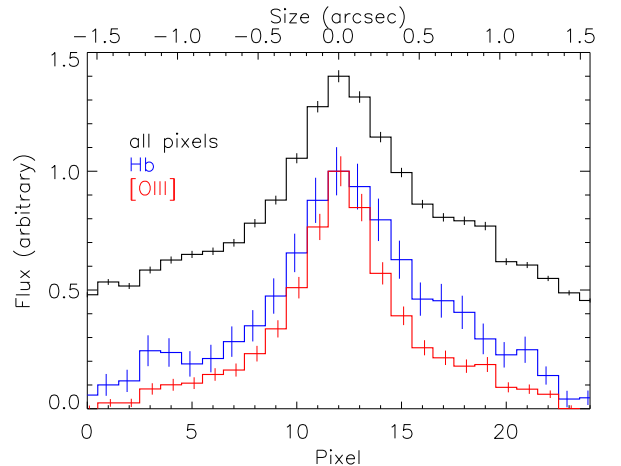


Fig. 5.— Spatial profiles of the Hβ (blue line) and [O III] (red line) emission lines, along with the entire spectrum (black line, offset by +0.4 in flux). Each 1D profile is extracted along the cross-dispersion direction, using the three pixels (140Å) about each line center for the emission lines or the entire wavelength range for the entire spectrum profile. The Hβ profile is more extended than the [O III] profile with 98.1% confidence, suggesting that at least some of the objects have a compact AGN contributing to the [O III] emission.

the [O III] line is more compact than the Hβ line with 98.1% confidence.

We also measure the spatially resolved $f([O III])/f(Hβ)$ ratio and $(U - B)$ in the inner and outer regions of the stacked spectrum. We designate the "inner region" as the central $3 \times 3$ pixel box ($0.''39 \times 0.''39$, or $3.2 \times 3.2$ kpc at $z = 1.86$) in the cross-dispersion direction, and the "outer region" as the two boxes 3 pixels wide from pixel numbers 4 through 6 ($0.''39 - 0.''78$) above and below the
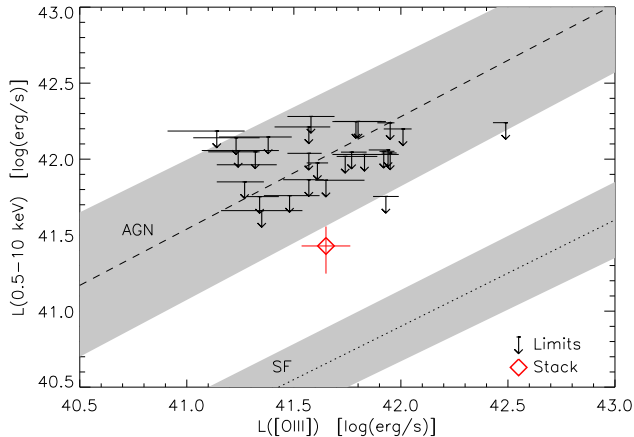
FIG. 6.— X-ray luminosity with [O III] luminosity for the 28 $z \sim 2$ galaxies from the WFC3 G141 data. Since all of our galaxies are undetected in X-rays, we show them as X-ray upper limits. The red diamond shows the stacked X-ray data (and mean $L_{[OIII]}$) for the sample. The dashed line shows the typical relation between $L_X$ and $L_{[OIII]}$ for Type 2 AGNs (LaMassa et al. 2011) and the dotted line shows the typical relation for star-forming galaxies (Rovilos et al. 2009), both at $z \sim 0$, with the $1\sigma$ scatter about each relation indicated by the gray shaded area. The position of the stacked X-ray data in $L_X - L_{[OIII]}$ space suggests that an AGN is present in at least some of the galaxies.

center in the cross-dispersion direction. Line ratios are calculated for both the inner and outer regions, using the same method of continuum subtraction and Gaussian fitting described above.

Color gradients were calculated using the CANDELS WFC3 $Y$, $J$, and $H$ imaging (Koekemoer et al. 2011). The WFC3 images are drizzled to a finer resolution (0″.06) than the WFC3 spectroscopy, and so we adopt 0″.36 (6 pixel circular diameter) as the inner region and 0″.36 − 0″.72 (circular annulus from 6 to 12 pixels) as the outer region. Rather than stacking, we measure aperture $Y$, $J$, and $H$ for each individual galaxy. We then treat the median $Y - J$ (for low redshift $z < 1.8$) or $J - H$ (for $z > 1.8$) difference from the inner ($< 0″.36$) to outer (0″.36 − 0″.72) aperture as the change in $(U - B)_{rest}$ over the same aperture.

As Figure 4 shows, the stacked inner region has marginally redder colors and slightly higher line ratios than the outer region. In other words, the inner region is more like an AGN than the outer region. However the large errors (particularly on the outer ratio) mean that this is significant only at the $1.0\sigma$ level (67%). This is probably because the 0″.39 size of the inner region corresponds to the inner 3.2 kpc of the galaxy (at the median redshift $z = 1.86$), and so includes much more than the typical $\sim 1$ kpc narrow line region (NLR) of an AGN. The marginal difference between inner and outer line ratios is merely suggestive, but is reinforced by the far more significant (98.1% confidence) result that the [O III] profile is more compact than H$\beta$.

### 3.2. *Stacked Chandra Data*

In Figure 6 we show the full-band (observed 0.5-10 keV) X-ray luminosity upper limits with the [O III]$\lambda$5007 emission line luminosity. The dashed line

shows the typical $L_X - L_{[OIII]}$ relation for [O III]-selected narrow-line AGN (LaMassa et al. 2011), with associated $1\sigma$ scatter of $\sim 0.5$ dex indicated by the gray shaded area, and the dotted line shows the typical $L_X - L_{[OIII]}$ relation for star-forming galaxies (Rovilos et al. 2009), with the gray shaded area similarly indicating the $1\sigma$ scatter of $\sim 0.3$ dex.

We stack the X-ray data for the undetected sources to learn whether the population has $L_X - L_{[OIII]}$ dominated by black hole activity or star formation. The stacked data is marginally detected ($2.9\sigma$ significant) with a flux of $f_{0.5-10 \mathrm{keV}} = 1.1 \times 10^{-17}$ erg s$^{-1}$ cm$^{-2}$. At the median redshift of our sample, $z = 1.86$, this translates to an X-ray luminosity of $L_{0.5-10 \mathrm{keV}} = 2.7 \times 10^{41}$ erg s$^{-1}$. Because the stack is only marginally detected in the full band, we cannot comment on its hardness. Unless the typical $L_X - L_{[OIII]}$ relation for star formation changes with redshift, the position of the stacked data is intermediate between the loci of AGN and star formation. This suggests that at least some of the galaxies have an AGN contributing to the [O III] and X-ray emission.

### 4. NATURE OF $Z \sim 2$ EMISSION-LINE GALAXIES

The stacked set of our $z \sim 2$ galaxies shows a more compact [O III] profile than the H$\beta$ emission line. This is the reverse of what is expected for typical galaxy metallicity gradients (van Zee et al. 1998), but is expected if an AGN in the galaxy's center contributes to the line emission. We find a marginally higher [O III]/H$\beta$ in the center of the stacked data, similar to the higher-confidence result of Wright et al. (2010), who found a steeper [O III]/H$\beta$ ratio in the center of one $z = 1.6$ galaxy. In addition the stacked *Chandra* data suggests an AGN component in at least some objects, since the position of the stacked data in $L_X - L_{[OIII]}$ is intermediate between the lines of star formation and black hole activity. For these reasons we suggest that some of these $z \sim 2$ emission-line galaxies, and those with similar line ratios and colors from other authors (Shapley et al. 2005b; Erb et al. 2006; Kriek et al. 2007), probably contain weak AGN in their centers.

Because we rely on stacked data to reveal an AGN, it is difficult to know the frequency of nuclear activity in these galaxies. In the local universe, AGN activity is known to correlate with SFR (e.g. Shi et al. 2009), so AGN activity might be expected in our galaxies given their bright emission lines and presumably high star formation rates. While some authors have argued that AGN are rare in local galaxies with $M_* < 10^{10} M_\odot$ (Kauffmann et al. 2003), recent work suggests instead that AGN incidence is constant with host mass at $z < 1$ (Aird et al. 2011). Our sample has a median mass of $M_* = 10^{9.5} M_\odot$, and so unless a few massive objects are dominating the stacked X-ray and grism spectrum, this suggests that AGN are common in low-mass star-forming galaxies at $z \sim 2$.

REFERENCES

Aird, J. et al. 2011, ApJ in press (arXiv:1107.4368)
Alexander, D. M., Chartas, G., Bauer, F. E., Brandt, W. M., Simpson, C. & Vignali, C. 2005, MNRAS, 357, 16
Alexander, D. M. et al. 2008, ApJ, 687, 835
Baldwin, J. A., Phillips, M. M. & Terlevich, R. 1981, PASP, 93, 5
Beckwith, S. V. W. et al. 2006, AJ, 132, 1729
Bell, E. F. et al. 2011, in prep
Blanton, M. R. & Roweis, S. 2007, AJ, 133, 734
Brinchmann, J., Pettini, M. & Charlot, S. 2008, MNRAS, 385, 769
Calzetti, D. 2001, PASP, 113, 1449
Cardamone, C. N. et al. 2010, ApJ, 189, 270
Daddi, E. et al. 2007, ApJ, 670, 173
Erb, D. K., Shapley, A. E., Pettini, M., Steidel, C. C., Reddy, N. & Adelberger, K. L. 2006, ApJ, 644, 813
Erb, D. K., Pettini, M., Shapley, A. E., Steidel, C. C., Law, D. R. & Reddy, N. 2006, ApJ, 719, 1168
Erlund, M. C., Fabian, A. C., Blundell, K. M. & Crawford, C. S. 2008, MNRAS, 385, 125
Finkelstein, S. L. et al. 2011, ApJ, 729, 140
Fioc, M. & Rocca-Volmerange, B. 1997, A&A, 326, 950
Fiore, F. et al. 2009, ApJ, 693, 447
Garmire, G. P., Bautz, M. W., Ford, P. G., Nousek, J. A. & Ricker, G. R., Jr. 2003, SPIE, 4851, 28
Gawiser, E. et al. 2006, ApJS, 162, 1
Georgantopoulos, I., Rovilos, E., Xilouris, E. M., Comastri, A. & Akylas, A. 2011, A&A, 526, 86
Gilli, R., Comastri, A. & Hasinger, G. 2007, A&A, 463, 79
Grazian, A. et al. 2006, A&A, 449, 951
Grogin, N. A. et al. 2011, ApJ submitted (arXiv:1105.3753)
Hayashi, M. et al. 2009, ApJ, 691, 140
Izotov, Y. I. & Thuan, T. X. 2008, ApJ, 687, 133
Juneau, S., Dickinson, M., Alexander, D. M. & Salim, S. 2011, ApJ in press (arXiv:1105.3194)
Kauffmann, G. et al. 2003, MNRAS, 346, 1055
Kennicutt, R. C., Jr. 1998, ARA&A, 36, 189
Kewley, L. J., Dopita, M. A., Sutherland, R. S., Heisler, C. A. & Trevena, J. 2001, ApJ, 556, 121
Kewley, L. J., Groves, B., Kauffmann, G. & Heckman, T. 2006, MNRAS, 372, 961
Koekemoer, A. et al. 2011, ApJ submitted (arXiv:1105.3754)
Kriek, M. et al. 2007, ApJ, 669, 776
Kümmel, M., Walsh, J. R., Pirzkal, N., Kuntschner, H. & Pasquali, A. 2009, PASP, 121, 59
Laird, E. S. et al. 2009, ApJS, 180, 102

Lamassa, S. M., Heckman, T. M., Ptak, A., Martins, L., Wild, V., Sonnentrucker, P. & Hornschemeier, A. 2011, ApJ, 729, 52
Liu, X., Shapley, A. E., Coil, A. L., Brinchmann, J. & Ma, C.-P. 2008, ApJ, 678, 758
Martinez-Sansigre, A. et al. 2007, ApJ, 379, 6
Mignoli, M. et al. 2005, A&A, 437, 883
Onodera, M., Arimoto, N., Daddi, E., Renzini, A., Kong, X., Cimatti, A., Broadhurst, T. & Alexander, D. M. 2010, ApJ, 715, 385
Papovich, C., Dickinson, M., Giavalisco, M., Conselice, C. J., & Ferguson, H. C. 2005, ApJ, 631, 101
Polletta, M. et al. 2007, ApJ, 663, 81
Reddy, N. A. et al. 2006, ApJ, 644, 792
Rodney, S. A. et al. 2011, in prep.
Rovilos, E., Georgantopoulos, I., Tzanavaris, P., Pracy, M., Whiting, M., Woods, D. & Goudis, C. 2009, A&A, 502, 85
Ryan, R. E. Jr. et al. 2007, ApJ, 668, 839
Santini, P. et al. 2009, A&A, 504, 751
Shapley, A. E., Erb, D. K., Pettini, M., Steidel, C. C. & Adelberger, K. L. 2004, ApJ, 612, 108
Shapley, A. E., Steidel, C. C., Erb, D. K., Reddy, N., Adelberger, K. L., Pettini, M., Barmby, P. & Huang, J. 2005a, ApJ, 626, 698
Shapley, A. E., Coil, A. L., Ma, C.-P. & Bundy, K. 2005b, ApJ, 635, 1006
Shi, Y., Rieke, G. H., Ogle, P., Jiang, L. & Diamond-Stanic, A. M. 2009, ApJ, 703, 1107
Shim, H., Chary, R.-R., Dickinson, M., Lin, L., Spinrad, H., Stern, D., & Yan, C.-H. 2011, ApJ submitted (arXiv:1103.4124)
Storey, P. J. & Zeippen, C. J. 2000, MNRAS, 312, 813
Straughn, A. N. et al. 2008, AJ, 135, 1624
Straughn, A. N. et al. 2011, AJ, 141, 14
Treister, E., Urry, C. M. & Virani, S. 2009, ApJ, 696, 110
Vanzella, E. et al. 2008, A&A, 478, 83
van der Wel, A. et al. 2011, in prep
van Zee, L., Salzer, J. J., Haynes, M. P., O'Donaghue, A. A. & Balonek, T. J. et al. 1998, AJ, 116, 2805
Veilleux, S. & Osterbrock, D. E. 1987, ApJ, 63, 295
Wolf, C. et al. 2004, A&A, 421, 913
Wright, S. A., Larkin, J. E., Graham, J. R. & Ma, C.-P. 2010, ApJ, 711, 1291
Wuyts, S., Labbé, I., Förster Schreiber, N. M., Franx, M., Rudnick, G., Brammer, G. B. & van Dokkum, P. G. 2008, ApJ, 682, 985
Yan, R. et al. 2011, ApJ, 728, 38
Yuan, T.-T. & Kewley, L. J. 2009, ApJ, 699, 161